Attospin and channel closings in high-order above-threshold ionization by bicircular laser fields

D. B. Milošević

Faculty of Science, University of Sarajevo, Zmaja od Bosne 35, 71000 Sarajevo, Bosnia and Herzegovina; Academy of Sciences and Arts of Bosnia and Herzegovina, Bistrik 7, 71000 Sarajevo, Bosnia and Herzegovina; and Max-Born-Institut, Max-Born-Str. 2a, 12489 Berlin, Germany

(Received 15 August 2018; published 15 November 2018)

In Phys. Rev. A **93**, 051402(R) (2016), we proposed a method to introduce spin into attoscience with spin-polarized electrons produced by a bicircular laser field. In the present paper we further develop this method. We calculate focal-averaged photoelectron spectra and the corresponding spin asymmetry parameter by using the improved strong-field approximation. We show that the spin asymmetry of the rescattered electrons, which is time dependent on the attosecond timescale, can become especially large for particular peak laser intensities. The pertinent jumps in the spin asymmetry occur when the peak intensity changes so that certain above-threshold ionization channel-closing intensities corresponding to the different ionization continua of Xe become covered by the intensity distribution.

DOI: 10.1103/PhysRevA.98.053420

I. INTRODUCTION

The dynamics of electrons in atoms, molecules, and solids develops on the attosecond timescale. Attoscience, which is developed based on the achievements of strong-field physics, is nowadays able to govern this dynamics [1]. In particular, in strong-field-ionization processes, the rescattering of temporarily liberated electrons off the parent ion happens during a small part of the driving-laser-field optical cycle and thus, by using standard femtosecond lasers, one can easily reach the attosecond timescale [2]. On the other hand, the electrons have an intrinsic property—spin $\frac{1}{2}$. Introduced in physics in early 1920s with the Stern–Gerlach experiment [3] and the Uhlenbeck and Goudsmit hypothesis [4], spin governs the behavior of matter, from the periodic table to magnetism. The Stern–Gerlach method cannot be used to obtain spin-polarized electrons. Fano was the first who suggested to obtain such electrons by photoionization of nonpolarized atoms by circularly polarized light [5]. Later on, Lambropoulos generalized this method to multiphoton ionization [6]. Spin-polarized electrons have many applications (for reviews see Refs. [7–9]).

In strong-field physics the influence of the electron spin has been neglected until recently. It was proposed in Ref. [10] to generate spin-polarized electrons in the ionization of inert atomic gases having a p ground state by using a circularly polarized strong laser field (see also Refs. [11–13]). This has recently been realized experimentally in strong-field ionization of Xe atoms [14–16]. It is well known that the rescattering in circularly polarized laser field is negligible. If one wants to explore the spin-polarized electrons on the attosecond timescale new methods should be discovered. In Ref. [17] we proposed to use a bicircular laser field for this purpose. A bicircular laser field consists of two coplanar counter-rotating circularly polarized fields of different frequencies (usually ω and 2ω; see the inset of Fig. 1). A bicircular field provides a strong asymmetry in ionization rates from the atomic ground states having opposite values of the magnetic quantum number ($m = +1$ and $m = -1$), which is necessary for generation of spin-polarized electrons. Furthermore, a bicircular field allows rescattering. This was confirmed much earlier in high-order harmonic generation experiments [18]. The returning electron trajectories were identified in Ref. [19]. High-order harmonic generation by bicircular fields is currently a very active area of research, mainly because the generated harmonics are circularly polarized and have many applications [20,21]. The generation of ultrashort elliptically and circularly polarized pulses of high harmonics is based on the mentioned $m = \pm 1$ asymmetry of ionization and recombination amplitudes which govern high-order harmonic generation process [22,23].

Spin-polarized electrons can be obtained in the strong-field ionization of atoms having a fine-structure splitting. For example, for Xe atoms there are two continua corresponding to two ground states of Xe^+ ions ($^2P_{3/2}$ and $^2P_{1/2}$) which have a fine-structure splitting of 1.31 eV. The spectrum of electrons liberated in above-threshold ionization (ATI) consists of discrete peaks at the energies ${E_{\mathbf{p}}}^j = n\hbar\omega - {I_p}^j - U_p$, where $n\hbar\omega$ is the energy absorbed from the laser field, $U_p = \langle \mathbf{A}^2(t)\rangle_T/2$ is the electron ponderomotive energy [energy of the electron in the laser electric field $\mathbf{E}(t) = -d\mathbf{A}(t)/dt$ averaged over the laser field period T], and ${I_p}^j$ is the ionization potential of the jth atomic ground state. Since n is integer, U_p is fixed for the fixed laser intensity, and ${I_p}^j$ is different for different j, so the ATI peaks appear at different positions for different j. The results for spin asymmetry, presented in Refs. [17,24], were obtained for fixed laser intensity. The overlap of the energies ${E_{\mathbf{p}}}^j$, which is necessary for calculation of the spin asymmetry parameter, was achieved by using the saddle-point method in which the energy $n\hbar\omega$ is a continuous parameter. However, in real experiments the laser intensity is a continuous parameter and the final results should be averaged over the spatial (laser focus) and temporal (laser pulse) intensity distributions. By applying focal averaging it is no longer necessary to use the saddle-point approximation and one can use more precise methods for calculating the ATI spectra, such as the improved strong-field

approximation (ISFA; for the bicircular-field case see Ref. [25]). More important is the fact that a continuous change of the laser intensity allows exploration of the influence of the so-called channel-closing effect on the generation of spin-polarized electrons. Namely, with increasing laser intensity, for some laser intensity the absorption of the energy $n\hbar\omega$ from the laser field is no longer sufficient for ionization and the energy $(n+1)\hbar\omega$ is required (recall that the electron kinetic energy ${E_{\mathbf{p}}}^{j} = n\hbar\omega - {I_p}^{j} - U_p$ must be positive). In this case we say that the channel which corresponds to the energy $n\hbar\omega$ is closed. It should be mentioned that, since $U_p \propto I\lambda^2$, where I and λ are, respectively, the laser intensity and wavelength, the channel closing can also be achieved by increasing the laser wavelength.

More details about the channel-closing effect can be found in recent topical review [26] and references therein. Channel closings for the bicircular-field case have also been considered recently in Ref. [27], where it was confirmed that the resonant-like enhancements in high-order ATI (HATI) spectra appear not only for a linearly polarized laser field but also for a bicircular field. In the present paper we explore how the channel-closing mechanism influences spin-polarized electrons and in particular rescattered spin-polarized electrons responsible for attospin. We use atomic units $\hbar = m_e = e = 1$ throughout the paper.

II. THEORY

For a laser field having the peak intensity $I_{\max}$, the focal-averaged differential electron ionization yield is proportional to [28–32]

$$\sum_n x\sqrt{\ln x}\, w_{\mathbf{p}i}(n), \tag{1}$$

where $x = U_{p,\max}/U_p$, with $U_p = n\omega - E_{\mathbf{p}} - I_p$, and the sum extends over integer n from the interval $(E_{\mathbf{p}} + I_p)/\omega < n < (E_{\mathbf{p}} + I_p + U_{p,\max})/\omega$. The result (1) was obtained in the weak-focusing approximation. For our counter-rotating bicircular $r\omega$-$s\omega$ field and equal component intensities $I = I_1 = I_2$, the ponderomotive energy is $U_p = I_1/(2r\omega)^2 + I_2/(2s\omega)^2 = (r^{-2} + s^{-2})I/(2\omega)^2$. The ponderomotive energy $U_{p,\max}$ corresponds to the peak intensity $I = I_{\max}$.

In Eq. (1) $w_{\mathbf{p}i}(n) = 2\pi p|T_{\mathbf{p}i}(n)|^2$ is the differential ionization rate of atoms having the initial ground state ψ_i with the ionization potential I_p, by a $T = 2\pi/\omega$-periodic bicircular laser field, with emission of an electron with momentum $\mathbf{p}$ and energy $E_{\mathbf{p}} = \mathbf{p}^2/2$, and with absorption of the energy $n\omega$ from the laser field. Within the improved strong-field approximation, the T-matrix element $T_{\mathbf{p}i}(n)$ is presented as a sum of the direct and rescattering T-matrix elements which are calculated numerically integrating over the ionization and rescattering times, as it is described in Ref. [25]. In Ref. [17] the rates were calculated in the saddle-point approximation and without focal averaging.

The index i denotes the orbital quantum number ℓ, magnetic quantum number m, and the ionization potential of the atomic ground state. For Xe atoms, which we will consider, the ground state is p state so that $\ell = 1$ and $m = \pm 1$ (matrix elements are zero for $m = 0$). For ionization of Xe atoms there are two continua corresponding to two ground states of Xe^+ ions ($^2P_{3/2}$ and $^2P_{1/2}$) so that we have two ionization potentials ${I_p}^{3/2} = 12.13$ eV and ${I_p}^{1/2} = 13.44$ eV. The same is valid for Kr atoms but the corresponding fine-structure splitting is smaller and so are the spin asymmetry effects that we are exploring. We denote the rate by $w_{\mathbf{p},m,j}$ where $m = \pm 1$ and $j = 3/2$ for ${I_p}^{3/2}$ and $j = 1/2$ for ${I_p}^{1/2}$ [this is shorter notation than the notation $w_{\mathbf{p}il}^{(m,m_s)}({I_p}^{j})$ used in Ref. [17]]. For the differential ionization rate for electrons with spin up ($W_{\mathbf{p}\uparrow}$) and spin down ($W_{\mathbf{p}\downarrow}$) we obtain

$$W_{\mathbf{p}\uparrow} = \tfrac{1}{3}\left(2w_{\mathbf{p},-1,\frac{1}{2}} + w_{\mathbf{p},-1,\frac{3}{2}}\right) + w_{\mathbf{p},1,\frac{3}{2}}, \tag{2}$$

$$W_{\mathbf{p}\downarrow} = \tfrac{1}{3}\left(2w_{\mathbf{p},1,\frac{1}{2}} + w_{\mathbf{p},1,\frac{3}{2}}\right) + w_{\mathbf{p},-1,\frac{3}{2}}. \tag{3}$$

For presentation in the momentum plane we use the spin asymmetry parameter $A_{\mathbf{p}}$ and the normalized spin asymmetry parameter $\tilde{A}_{\mathbf{p}}$ (with respect to the maximal summed rate) defined by the relations

$$A_{\mathbf{p}} = (W_{\mathbf{p}\uparrow} - W_{\mathbf{p}\downarrow})/W_{\mathbf{p}}, \quad \tilde{A}_{\mathbf{p}} = A_{\mathbf{p}}\tilde{W}_{\mathbf{p}}, \tag{4}$$

where $W_{\mathbf{p}} = W_{\mathbf{p}\uparrow} + W_{\mathbf{p}\downarrow}$ and $\tilde{W}_{\mathbf{p}} = W_{\mathbf{p}}/\max_{\mathbf{p}} W_{\mathbf{p}}$ is the normalized summed rate. If ${I_p}^{1/2} = {I_p}^{3/2}$, i.e., if we neglect the spin-orbit coupling, then from Eqs. (2)–(4) it follows that $A_{\mathbf{p}} = 0$. In our case of Xe atoms the fine-structure splitting is ${I_p}^{1/2} - {I_p}^{3/2} = 1.31$ eV and we expect a substantial spin asymmetry. If the rates are the same for $m = +1$ and $m = -1$ then the asymmetry parameter $A_{\mathbf{p}}$ is also zero. However, for ATI of inert gases having a p ground state by a circularly polarized laser field [10–16] and for (H)ATI by a bicircular field [22,23], the ionization rate exhibits strong $m = \pm 1$ asymmetry, so that for Xe we expect large values of $A_{\mathbf{p}}$. Furthermore, for a bicircular field electron rescattering is possible, which opens up access to attosecond spin effects [17,24].

When the laser intensity or its wavelength increases, at some point the absorption of energy $N\omega$ from the laser field is no longer sufficient for ionization and energy $(N+1)\omega$ is required. In this case we say that the channel N is closed. This is the so-called channel-closing phenomenon (see Refs. [26,27] and references therein). At the values of the laser parameters which correspond to channel closing one can expect sharp features and the enhancement in the spectra. For our bicircular field we expect enhancements for channel-closing intensities $I_{n_c}^{j}$ which satisfy the condition

$$n_c\omega = {I_p}^{j} + U_p\left(I_{n_c}^{j}\right). \tag{5}$$

From this we obtain

$$I_{n_c}^{j} = \frac{r^2 s^2}{r^2 + s^2}\left(n_c\omega - {I_p}^{j}\right)4\omega^2. \tag{6}$$

For a pulse with peak intensity $I_{\max}$ and the corresponding ponderomotive energy $U_{p,\max}$ the relevant values of n_c are from $n_{c,\min} = [{I_p}^{j}/\omega] + 1$ to $n_{c,\max} = [({I_p}^{j} + U_{p,\max})/\omega]$. Exactly at a channel closing, the electron energy spectrum consists of peaks at the energies $E_{\mathbf{p}} = (n - n_{c,\min})\omega$, $n \geqslant n_{c,\min}$.

In Ref. [27] we considered two different manifestations of channel closings. First, in the total ionization yield, which

is dominated by low-energy (direct) electrons, we observed threshold anomalies and intensity-dependent enhancements and explained them with the help of the Wigner threshold law and conservation of energy and angular momentum. Calculations have been done for negative ions. For ionization of neutral atoms calculations show that the role of the excited states can be important (see, for example Ref. [33] where time-dependent Schrödinger equation has been solved numerically, and Ref. [34] where Floquet theory was used; see also references cited therein). The second manifestation of the channel closings is in the differential ionization yield of high-energy electrons [35]. For a laser intensity high enough that a sufficiently long plateau in the electron energy spectrum can develop, in the middle of the rescattering plateau resonant-like enhancements of groups of high-energy above-threshold ionization peaks at channel-closing intensities have been observed. One of the explanation of these enhancements is based on the quantum-orbit theory. Namely, near a channel closing electrons can be released with very low kinetic energy so that they may revisit their parent ion very often. It was shown [31] that the contributions of most of the corresponding quantum orbits interfere constructively, leading to the mentioned enhancements. These channel-closing enhancements can also be explained by using the threshold anomalies of scattering theory. Another quantum-mechanical explanation is that the enhancements occur at particular intensities where the laser-dressed ground atomic state is in resonance with some laser-dressed excited states (see the above-cited papers and the review article [26], and references therein).

We present results for (H)ATI of Xe atoms by ω-2ω bicircular field for which $r^2s^2/(r^2+s^2)=4/5$. The component intensities are equal $I_1=I_2$ and expressed in units $I_0=10^{14}$ W/cm^2. For the fundamental wavelength of 800 nm the corresponding channel-closing intensities $I_{n_c}^j$ are $I_{12}^{3/2}=0.866I_0$, $I_{13}^{3/2}=1.073I_0$, $I_{14}^{3/2}=1.281I_0$, $I_{12}^{1/2}=0.690I_0$, $I_{13}^{1/2}=0.898I_0$, and $I_{14}^{1/2}=1.105I_0$. We show the results for the peak intensities $I_{\max}=I_0$ and $I_{\max}=1.1I_0$. For $I_{\max}=I_0$ the enhancement is possible for $I=I_{n_c}\leqslant I_0$ which is satisfied for $n_c\leqslant 12$ for $j=3/2$ and for $n_c\leqslant 13$ for $j=1/2$. For $I_{\max}=1.1I_0$, both for $j=1/2$ and $j=3/2$, the enhancement is possible for $n_c\leqslant 13$.

We also present results for the fundamental wavelength of 1800 nm. In this case, for $I_{\max}=I_0$, we have $U_{p\max}=54.9\omega$, with $\omega=0.6888$ eV, and the enhancement is possible for $n_c\leqslant 72$ for $j=3/2$ and for $n_c\leqslant 74$ for $j=1/2$. The intensity interval between the subsequent channel closing intensities is $0.0182I_0$. Therefore, with a 2% change of the peak intensity one can exclude particular values of n_c.

III. DIRECT ABOVE-THRESHOLD IONIZATION

We first present results for direct ATI for the peak component intensities $I_1=I_2=I_0$ and the fundamental wavelength of 800 nm. In this case we have $U_{p\max}=4.82\omega$. From Fig. 1 we see that for fixed photoelectron emission angle $\theta=60^\circ$ the spin asymmetry parameter $A_{\mathbf{p}}$ changes rapidly with the photoelectron energy. This behavior was explained by the interference of the saddle-point solutions in Ref. [17]. It is interesting that the focal-averaged results obtained by

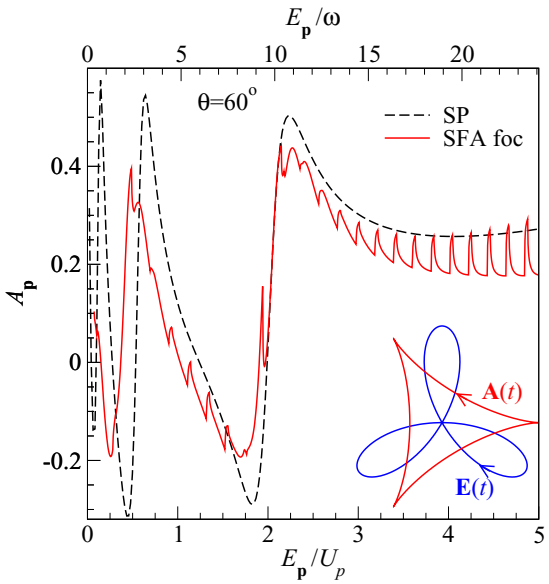

FIG. 1. Spin asymmetry parameter $A_{\mathbf{p}}$ as a function of the photoelectron energy $E_{\mathbf{p}}$ divided by the ponderomotive energy U_p (bottom) or by the fundamental photon energy ω (top). The field component peak intensities are $I_1=I_2=1\times10^{14}$ W/cm^2 and the fundamental wavelength is 800 nm. The electron emission angle is $\theta=60^\circ$. Results are obtained by using the saddle-point method for direct electrons [36] (black dashed curve) and by using the focal averaging and the strong-field approximation with numerical integration over the ionization time (red solid curve). In the lower-right panel we present parametric plot of our bicircular electric field vector $\mathbf{E}(t)$ and the corresponding vector potential $\mathbf{A}(t)$.

numerical integration (red solid curve) follow the same oscillatory structure as the saddle-point results (black dashed curve). Additional peaks in the focal-averaged spectra at distances approximately equal to ω are related to the channel-closing effect [26,27] [channel-closing condition is satisfied by one (or several) lower intensities, as it is specified at the end of previous section; we will consider this in more detail in the next section for rescattering HATI].

Let us now consider how the asymmetry parameter changes in the momentum plane. For the same parameters as in Fig. 1, in Fig. 2 we present the focal-averaged results for the normalized spin asymmetry parameter $\tilde{A}_{\mathbf{p}}$ and the spin asymmetry parameter $A_{\mathbf{p}}$. All results presented exhibit threefold symmetry, i.e., the symmetry with respect to rotation by the angle 120° around the axis perpendicular to the laser field polarization plane in which the photoelectrons are recorded. For direct ATI we have additional reflection symmetry with respect to the axes which are at the angles $\theta=60^\circ$, 180°, and 300° with respect to the abscissa (p_x axis). Similar results were obtained in Ref. [17]. The main finding is that the spin of the electrons emitted in a particular direction considerably changes with the electron energy. The corresponding spin asymmetry parameter changes from a large positive to a large negative value. Important is that we have shown here that these results survive focal averaging so that this effect can be observed in the experiment. For the intensities $I_1=I_2=I_0$ the spin asymmetry parameter changes from -0.4326 to 0.9525. We have calculated analogous results for the

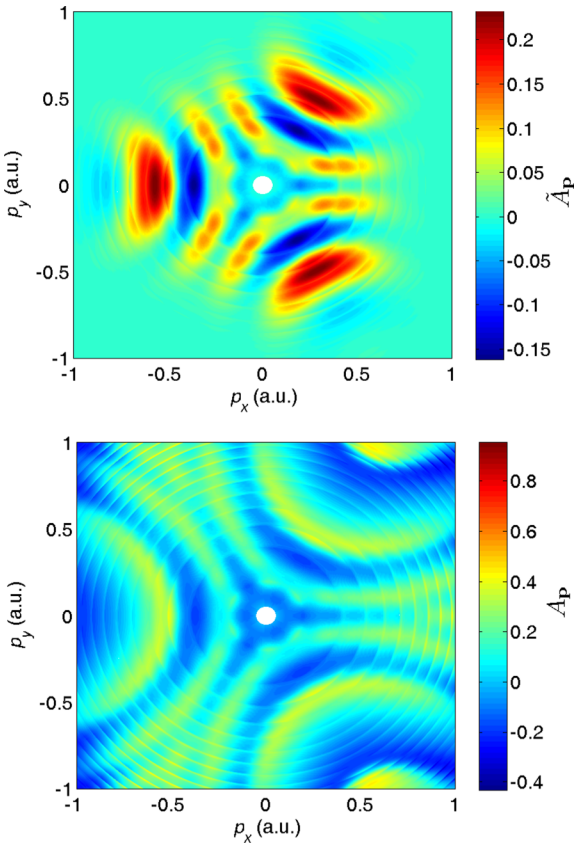

FIG. 2. Normalized spin asymmetry parameter $\tilde{A}_{\mathbf{p}}$ (upper panel) and the spin asymmetry parameter $A_{\mathbf{p}}$ (lower panel) for ATI of Xe atoms by bicircular ω-2ω field having the fundamental wavelength 800 nm and the peak component intensities $I_1 = I_2 = 1 \times 10^{14}$ W/cm^2. Results are obtained by using focal averaging and the SFA with numerical integration over the ionization time and are presented in false colors in the electron momentum plane.

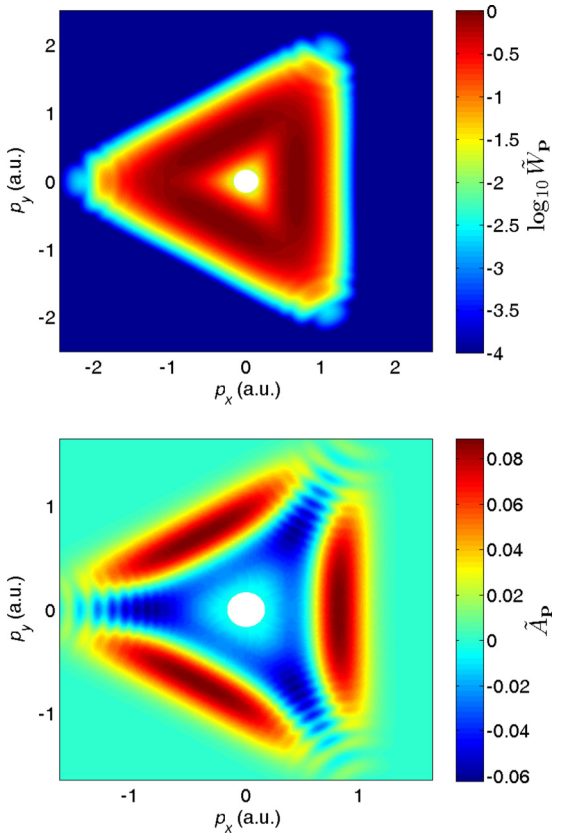

FIG. 3. The logarithm of the normalized summed photoelectron yield $\tilde{W}_{\mathbf{p}}$ (upper panel) and normalized spin asymmetry parameter $\tilde{A}_{\mathbf{p}}$ (lower panel) for ATI of Xe atoms by bicircular ω-2ω field having the fundamental wavelength 1800 nm and the peak component intensities $I_1 = I_2 = 1 \times 10^{14}$ W/cm^2. Results are obtained by using focal averaging and the SFA with numerical integration over the ionization time and are presented in false colors in the electron momentum plane.

intensities $I_1 = I_2 = 1.1I_0$ and obtained that the spin asymmetry parameter changes from -0.4999 to 0.9800.

In Fig. 3 we show the focal-averaged results for the fundamental wavelength of 1800 nm and the peak component intensities $I_1 = I_2 = I_0$. The summed photoelectron yield, shown in the upper panel, exhibits typical triangular shape and follows the symmetry of the negative vector potential $-\mathbf{A}(t)$ [25] (see the inset of Fig. 1). In the interval $p_x \in [0.55, 0.8]$ a.u. and $p_y \in [-1, 1]$ a.u. there is a belt-like-shaped region of high photoelectron yield. From the bottom panel Fig. 3 we see that the normalized spin asymmetry parameter $\tilde{A}_{\mathbf{p}}$ in this region changes from a negative to a positive value (for the corresponding spin asymmetry parameter $A_{\mathbf{p}}$ see the right-hand ordinate in Fig. 4). This behavior is caused by an asymmetry in the peak positions for the $m = \pm 1$ partial contributions to the differential ionization yield. This is clearly seen in Fig. 4.

Comparing the normalized spin asymmetry parameter, presented in the upper panel of Fig. 2 for wavelength of 800 nm and in the lower panel of Fig. 3 for wavelength of 1800 nm, we notice two main differences. The first one is that the oscillations of $\tilde{A}_{\mathbf{p}}$ in the momentum plane for the angle $\theta = 60^\circ$ are stronger for shorter wavelength $\lambda = 800$ nm (there is a drop in the maximum asymmetry parameter by a factor of two for $\lambda = 1800$ nm). The second difference is that for the longer wavelength of 1800 nm, belt-like structures, centered at $\theta = 0^\circ$, 120°, and 240°, develop. They are caused by the asymmetry in the peak positions for the $m = \pm 1$ contributions to the ionization yield which is larger for longer wavelengths (see Fig. 4).

IV. RESCATTERING HIGH-ORDER ABOVE-THRESHOLD IONIZATION

Let us now present the results obtained by using the ISFA which includes rescattering electrons and thus provides access to attospin. In Fig. 5 we present results for two peak component intensities, I_0 and $1.1I_0$, and the fundamental wavelength of 800 nm. We present separately focal-averaged differential ionization photoelectron yields $\sum_m w_{\mathbf{p},m,\frac{1}{2}}$ (blue bottom curves), $\sum_m w_{\mathbf{p},m,\frac{3}{2}}$ (red middle curves), and $W_{\mathbf{p}}$ (black top curves). Low-energy spectra correspond to direct electrons, while the rescattered electrons are responsible for the plateau and cutoff regions. One can notice sharp peaks for photoelectron energies equal to integer multiples of the

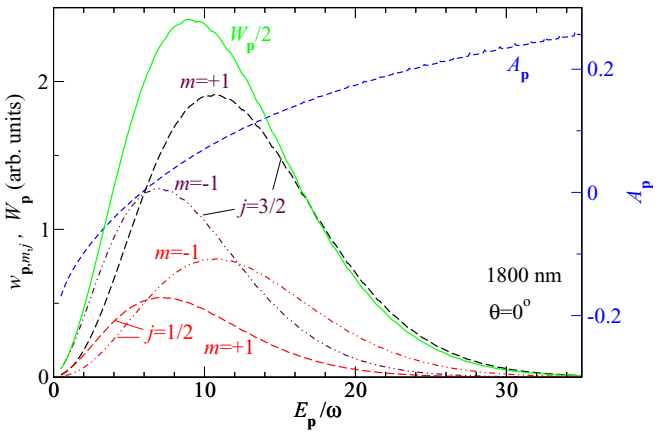

FIG. 4. The partial [$w_{\mathbf{p},m,j}$, $m = +1$ (long dashed lines) and $m = -1$ (double-dot dashed line); maroon lines are for $j = 3/2$ and red lines are for $j = 1/2$] and the total ($W_\mathbf{p}$, green solid line) focal-averaged photoelectron yields (in arb. units) and asymmetry parameter $A_\mathbf{p}$ (blue dashed line and right-hand ordinate) of Xe atoms as functions of the photoelectron kinetic energy $E_\mathbf{p}$ divided by ω for fixed electron emission angle $\theta = 0^\circ$, fundamental wavelength 1800 nm, and equal peak component intensities $I_1 = I_2 = 1 \times 10^{14}$ W/cm^2.

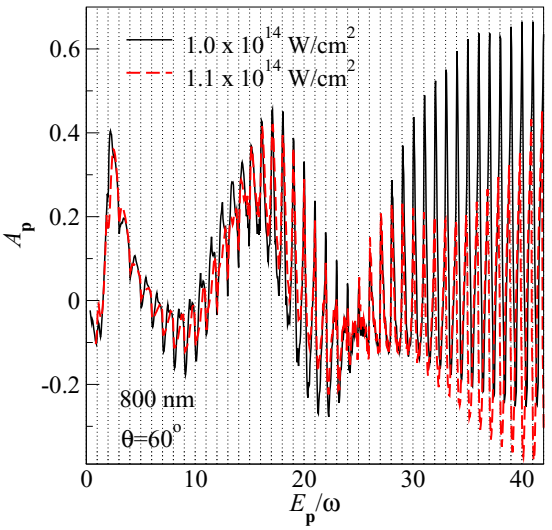

FIG. 6. Spin asymmetry parameter $A_\mathbf{p}$ as a function of the photoelectron energy divided by ω for the parameters of Fig. 5. In the high-energy region the values of $A_\mathbf{p}$ for the black solid curve are two to three times higher than that of the red dashed curve which corresponds to higher intensity.

fundamental frequency ω. The explanation of this effect is the following [26,27]: In general, the (H)ATI peaks are located at the energies $E_\mathbf{p} = k\omega - U_p - {I_p}^j$, with integer k. For the channel-closing intensities which satisfy the condition $n_c\omega = {I_p}^j + U_p$ we expect enhancements. The corresponding energy is $E_\mathbf{p} = (k - n_c)\omega$, which explains the position of the sharp peaks. For a particular peak intensity, there is a distribution of the intensities in the laser focus. For one (or several) of these lower intensities the resonant enhancement condition is satisfied. Nonresonant intensities also contribute to the process but the corresponding peaks are at different positions: $E_\mathbf{p} = k\omega - U_p - {I_p}^j$.

As we have mentioned, for the intensity $I_1 = I_2 = I_0$ the enhancement is possible for $n_c \leqslant 12$, while for $n_c = 13$ it is possible for ${I_p}^{1/2}$ but not for ${I_p}^{3/2}$. As a consequence, in the high-energy region ($E_\mathbf{p} > 25\omega$) in the left panel of Fig. 5 the bottom curve (for ${I_p}^{1/2}$) exhibits sharp peaks at $E_\mathbf{p} = (k - n_c)\omega$, contrary to the middle curve (for ${I_p}^{3/2}$) for which the enhancement is not possible for $n_c = 13$. Since the ionization probability for $j = 3/2$ state is higher, the sharp peaks in the summed yield (black top curve) are not visible for $E_\mathbf{p} > 25\omega$. However, for the intensity $1.1I_0$ (right panel of Fig. 5) the enhancement is possible for $n_c \leqslant 13$, both for $j = 1/2$ and $j = 3/2$, and the sharp peaks are clearly visible also in the summed spectrum.

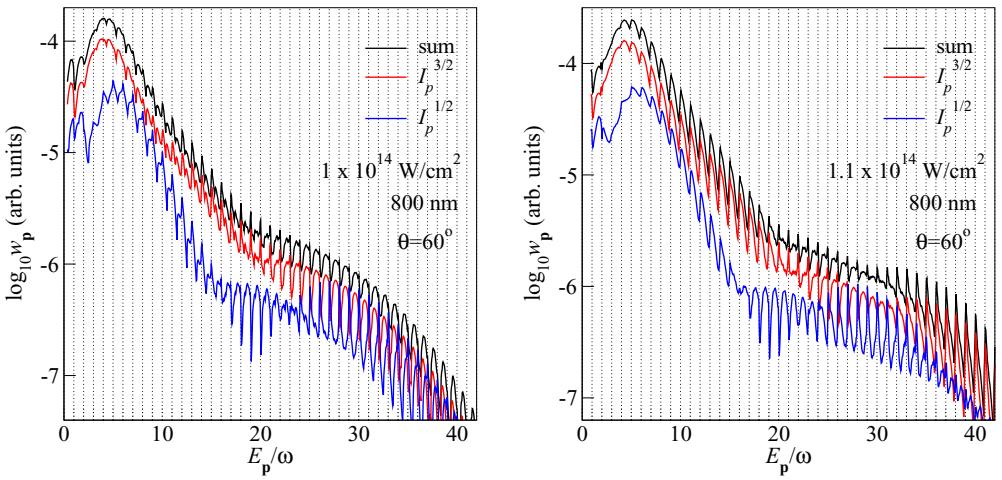

FIG. 5. The logarithm of the focal-averaged electron yield of Xe as a function of the photoelectron energy divided by ω. The ω-2ω bicircular laser field has the fundamental wavelength 800 nm and equal component intensities $I_1 = I_2 = 1 \times 10^{14}$ W/cm^2 (left panel) and $I_1 = I_2 = 1.1 \times 10^{14}$ W/cm^2 (right panel). The electron emission angle is $\theta = 60^\circ$. Presented results are for the summed photoelectron yield $W_\mathbf{p}$ (black top curves) and for the yield for ionization energies ${I_p}^{3/2} = 12.13$ eV (red middle curves) and ${I_p}^{1/2} = 13.44$ eV (blue bottom curves).

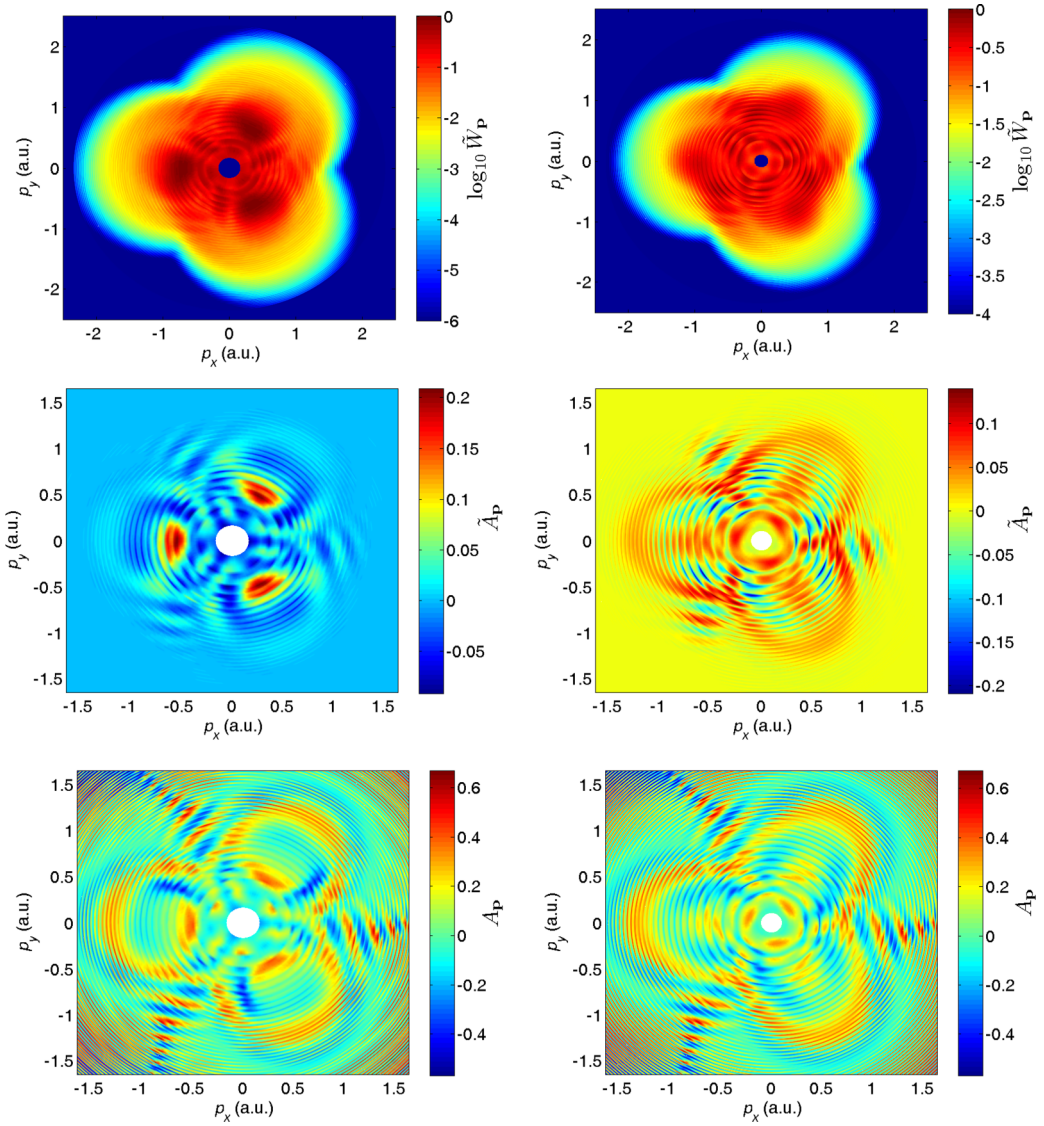

FIG. 7. Focal-averaged results for Xe atoms ionized by ω-2ω bicircular laser field having the fundamental wavelength of 800 nm and equal component intensities $I_1 = I_2 = 1 \times 10^{14}$ W/cm^2, presented in false colors in the photoelectron momentum plane: The logarithm of the normalized summed photoelectron yield $\tilde{W}_{\mathbf{p}}$ (upper panels), normalized spin asymmetry parameter $\tilde{A}_{\mathbf{p}}$ (middle panels), and spin asymmetry parameter $A_{\mathbf{p}}$ (lower panels). Left panels have both the direct and rescattered electrons taken into account. Right panels have only the rescattered electrons taken into account.

Let us now analyze how this channel-closing enhancement mechanism manifests in the results for spin asymmetry parameter. In Fig. 6 we see that in the region $E_{\mathbf{p}} > 25\omega$ the spin asymmetry parameter is larger by a factor of two to three for lower intensity for which the enhancement for $n_c = 13$ is not possible for the $j = 3/2$ case. For lower photoelectron energies the spin asymmetry parameters are comparable for both intensities. The conclusion is that we can control (and enhance) the spin asymmetry parameter by adjusting the laser intensity so that the enhancement is possible for a particular value of n_c for $j = 1/2$ but is not possible for $j = 3/2$. In the presented example this was achieved for a 10% difference in the intensity used, but this is also valid in a wider intensity interval [for example, 20% for $n_c = 13$ and 800 nm since $1.073/0.898 = 1.2$; see the second paragraph below Eq. (6)].

In Refs. [17,24] we presented photoelectron momentum distributions of the ionization rates and spin asymmetry parameters separately for the direct and rescattered electrons, obtained by using the saddle-point approximation. We were able to do this since, in the saddle-point method, the absorbed energy $n\omega$ is a continuous parameter so that we can combine the results for different states $j = 1/2$ and $j = 3/2$ (for integer n this would be impossible since the corresponding electron energies $E_{\mathbf{p}} = n\omega - U_p - {I_p}^j$ are different for fixed U_p and different j). In the present paper n is integer, but we have another continuous parameter—the laser intensity (and the corresponding ponderomotive energy). We obtain our SFA and ISFA results by numerical integration and we are able to present the results which (coherently) include both the direct and rescattered electrons (left panels in Fig. 7) and separate results which include only one of them (for example,

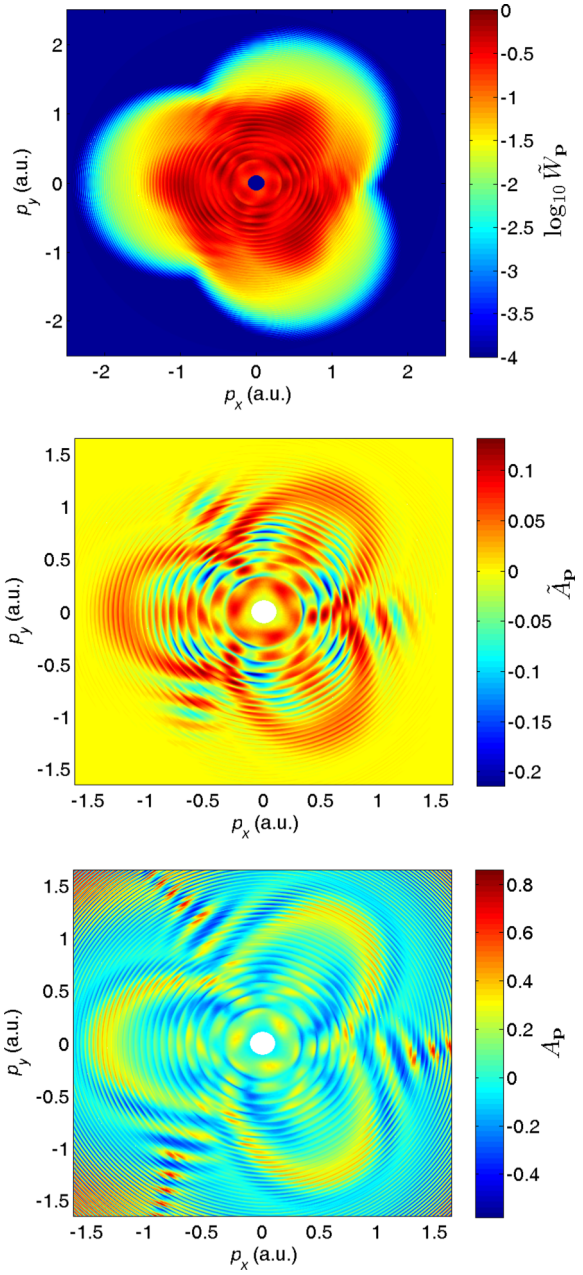

FIG. 8. Same as in right panels of Fig. 7 but for the component intensities 1.1×10^{14} W/cm^2.

in Figs. 1–3 we presented results for direct electrons, while in the right panels of Fig. 7 and in Fig. 8 only rescattered electrons are accounted for).

The summed electron yields, shown in the top panels of Fig. 7, exhibit threefold rotational symmetry, but do not show reflection symmetry since the rescattered electrons violate it. In the middle (bottom) panels of Fig. 7 we show the normalized spin asymmetry parameter $\tilde{A}_{\mathbf{p}}$ (spin asymmetry parameter $A_{\mathbf{p}}$). These results are for the peak component intensities equal to I_0. From the bottom panels we see that the spin asymmetry parameter has large values for high electron energies and emission angle of 60°, as in Fig. 6. We also see that this is valid in a wide range of energies and angles. The energy for which the spin asymmetry parameter has large

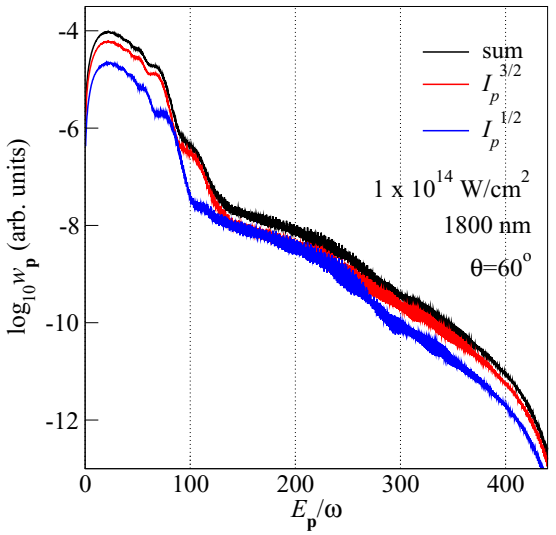

FIG. 9. The logarithm of the focal-averaged electron yield of Xe as a function of the photoelectron energy divided by ω for ionization by ω-2ω bicircular laser field having the fundamental wavelength 1800 nm and equal component intensities $I_1 = I_2 = 1 \times 10^{14}$ W/cm^2. The electron emission angle is $\theta = 60°$. We present the summed photoelectron yield $W_{\mathbf{p}}$ (black top curve), the yield for ionization energies $I_p{}^{3/2} = 12.13$ eV (red middle curve), and the yield for $I_p{}^{1/2} = 13.44$ eV (blue bottom curve).

values is maximal for $\theta = 60°$ and slowly decreases with the increase or decrease of θ. Analogous results for rescattered electrons, but for higher peak intensity $1.1I_0$, are shown in Fig. 8. Results are qualitatively similar to those presented in the right-hand panels of Fig. 7, but with less pronounced maxima of the spin asymmetry parameter.

Let us now consider HATI for longer wavelength of 1800 nm. In this case more channels are open. We expect that the plateau is the most pronounced for $\theta = 60°$. In Fig. 9, for ω-2ω bicircular laser field having equal component intensities $I_1 = I_2 = I_0$, we present results analogous to that shown in the left panel of Fig. 5, but for the wavelength of 1800 nm instead of 800 nm. We can distinguish three energy regions of the presented spectra. For $E_{\mathbf{p}} < 90\omega$ direct electrons are dominant, while for $E_{\mathbf{p}} > 120\omega$ rescattered electrons prevail. In the plateau region one can notice channel-closing enhancements. Since there are many such channels, the whole plateau in the energy region from 120ω to 260ω is enhanced. For the intensity $I_{\max} = I_0$ the enhancement can happen for all values $n_c \leqslant 72$. In addition, for $j = 1/2$ this happens also for $n_c = 73$ and $n_c = 74$ (corresponding channel-closing intensities are $I_{73}^{1/2} = 0.9743I_0$ and $I_{74}^{1/2} = 0.9925I_0$). As a consequence, in Fig. 9 the yield for the $j = 1/2$ case is more enhanced and the corresponding blue curve overlaps with the red curve which corresponds to $j = 3/2$. In the third region, for $E_{\mathbf{p}} > 300\omega$ channel-closing effect cannot be noticed and the yield for $j = 3/2$ is higher, as it should be since the corresponding ionization potential is lower than that of the $j = 1/2$ case.

V. CONCLUSIONS

Strong-field ionization of Xe atoms, having substantial fine-structure splitting, by a strong bicircular laser field

enables generation of rescattered spin-polarized electrons whose dynamics can be controlled on the attosecond timescale. This can open new directions in attosecond spectroscopy with high-order harmonic photons [20,21] or with high-energy electrons (laser-induced electron diffraction and holography [37,38]). We have explored spin polarization of these electrons by presenting the spin asymmetry parameter in the photoelectron momentum plane.

By averaging over the laser intensity distribution we emphasized the importance of the channel-closing effect. The channel-closing intensities are different for two different continua corresponding to $^2P_{3/2}$ and $^2P_{1/2}$ ground states of Xe^+ ion. By adjusting the peak laser intensity so that it comprises a particular set of channel-closing intensities we can control the spin asymmetry parameter. In the presented example we have shown an increase of the spin asymmetry parameter of the rescattered electrons by a factor two to three for a decrease of the peak intensity by 10% to 20%, which corresponds to the closing of the channel $n_c = 13$ for the $^2P_{3/2}$ state.

[1] F. Krausz and M. Ivanov, Rev. Mod. Phys. **81**, 163 (2009).

[2] D. B. Milošević, G. G. Paulus, D. Bauer, and W. Becker, J. Phys. B: At., Mol. Opt. Phys. **39**, R203 (2006).

[3] W. Gerlach and O. Stern, Z. Phys. **8**, 110 (1922); **9**, 349 (1922); **9**, 353 (1922).

[4] G. E. Uhlenbeck and S. Goudsmit, Nature (London) **117**, 264 (1926).

[5] U. Fano, Phys. Rev. **178**, 131 (1969); **184**, 250 (1969).

[6] P. Lambropoulos, Phys. Rev. Lett. **30**, 413 (1973); J. Phys. B **7**, L33 (1973); Adv. At. Mol. Phys. **12**, 87 (1976); S. N. Dixit, P. Lambropoulos, and P. Zoller, Phys. Rev. A **24**, 318 (1981); T. Nakajima and P. Lambropoulos, Europhys. Lett. **57**, 25 (2002).

[7] J. Kessler, *Polarized Electrons*, 2nd ed. (Springer-Verlag, Berlin, 1985).

[8] T. J. Gay, Adv. At. Mol. Opt. Phys. **57**, 157 (2009).

[9] I. Žutić, J. Fabian, and S. Das Sarma, Rev. Mod. Phys. **76**, 323 (2004).

[10] I. Barth and O. Smirnova, Phys. Rev. A **88**, 013401 (2013).

[11] T. Herath, L. Yan, S. K. Lee, and W. Li, Phys. Rev. Lett. **109**, 043004 (2012).

[12] I. Barth and O. Smirnova, Phys. Rev. A **87**, 065401 (2013).

[13] K. Liu, K. Renziehausen, and I. Barth, Phys. Rev. A **95**, 063410 (2017).

[14] A. Hartung *et al.*, Nat. Photonics **10**, 526 (2016).

[15] M.-M. Liu, Y. Shao, M. Han, P. Ge, Y. Deng, C. Wu, Q. Gong, and Y. Liu, Phys. Rev. Lett. **120**, 043201 (2018).

[16] D. Trabert, A. Hartung, S. Eckart, F. Trinter, A. Kalinin, M. Schöffler, L. Ph. H. Schmidt, T. Jahnke, M. Kunitski, and R. Dörner, Phys. Rev. Lett. **120**, 043202 (2018).

[17] D. B. Milošević, Phys. Rev. A **93**, 051402(R) (2016).

[18] H. Eichmann, A. Egbert, S. Nolte, C. Momma, B. Wellegehausen, W. Becker, S. Long, and J. K. McIver, Phys. Rev. A **51**, R3414 (1995).

[19] D. B. Milošević, W. Becker, and R. Kopold, Phys. Rev. A **61**, 063403 (2000).

[20] T. Fan *et al.*, Proc. Natl. Acad. Sci. U.S.A. **112**, 14206 (2015).

[21] C. Chen *et al.*, Sci. Adv. **2**, e1501333 (2016).

[22] D. B. Milošević, Opt. Lett. **40**, 2381 (2015); Phys. Rev. A **92**, 043827 (2015).

[23] L. Medišauskas, J. Wragg, H. van der Hart, and M. Yu. Ivanov, Phys. Rev. Lett. **115**, 153001 (2015).

[24] D. B. Milošević, J. Phys. B: At., Mol. Opt. Phys. **50**, 164003 (2017).

[25] D. B. Milošević and W. Becker, Phys. Rev. A **93**, 063418 (2016).

[26] W. Becker, S. P. Goreslavski, D. B. Milošević, and G. G. Paulus, J. Phys. B: At., Mol. Opt. Phys. **51**, 162002 (2018).

[27] D. B. Milošević and W. Becker, J. Phys. B: At., Mol. Opt. Phys. **51**, 054001 (2018).

[28] R. Kopold, W. Becker, M. Kleber, and G. G. Paulus, J. Phys. B: At., Mol. Opt. Phys. **35**, 217 (2002).

[29] D. B. Milošević, A. Gazibegović-Busuladžić, and W. Becker, Phys. Rev. A **68**, 050702(R) (2003); A. Gazibegović-Busuladžić, D. B. Milošević, and W. Becker, *ibid.* **70**, 053403 (2004).

[30] E. Hasović, M. Busuladžić, A. Gazibegović-Busuladžić, D. B. Milošević, and W. Becker, Laser Phys. **17**, 376 (2007).

[31] D. B. Milošević, E. Hasović, M. Busuladžić, A. Gazibegović-Busuladžić, and W. Becker, Phys. Rev. A **76**, 053410 (2007).

[32] D. B. Milošević, W. Becker, M. Okunishi, G. Prümper, K. Shimada, and K. Ueda, J. Phys. B: At., Mol. Opt. Phys. **43**, 015401 (2010).

[33] B. Piraux, F. Mota-Furtado, P. F. O'Mahony, A. Galstyan, and Yu. V. Popov, Phys. Rev. A **96**, 043403 (2017).

[34] K. Krajewska, I. I. Fabrikant, and A. F. Starace, Phys. Rev. A **86**, 053410 (2012).

[35] We consider only this manifestation in the present paper. It appears for a linearly polarized laser field and for a bichromatic circularly polarized field with corotating components (bicircular field). However, due to the absence of rescattering, it does not appear for a monochromatic circularly polarized field or for a bichromatic circularly polarized field with corotating components.

[36] The corresponding saddle-point results have already been presented in the lower-right panel of Fig. 3 in Ref. [17]. There was a numerical error in this calculation (error in the value of the constant A for the asymptotic wave function) but the results are qualitatively the same. We thank Xuanyang Lai from the Wuhan Institute of Physics and Mathematics, CAS, for noticing this.

[37] M. Meckel *et al.*, Science **320**, 1478 (2008).

[38] Y. Huismans *et al.*, Science **331**, 61 (2011).